Proceedings of ASME Turbo Expo 2011
GT2011
June 6-10, 2011, Vancouver, British Columbia, Canada

GT2011-46656

SIMULTANEOUS NOISE AND PERFORMANCE MEASUREMENTS FOR HIGH SPEED JET NOISE REDUCTION TECHNOLOGIES: PART II NEAR FIELD ARRAY CALIBRATION

Dean Long*
Aero Systems Engineering
St. Paul, MN 55107

Steve Martens
GE Global Research Center
Niskayuna, NY 12309

ABSTRACT

Part I of this paper describes a methodology for assessing the far field jet noise from high speed exhaust nozzles using a microphone array in the near field of the exhaust plume. The near field noise measurement is mathematically propagated producing an estimate of the noise level at the new location. Outward propagation produces an estimate of the far field noise. Propagation toward the jet axis produces the source distribution. Part II described here provides a direct validation of this process using a generic CD nozzle in a facility where both the near field and the far field are measured simultaneously. Comparison of these data sets show good agreement over the typical operating range for this type of nozzle. The far field noise is characterized by two independent processes: Shock cell noise radiating in the forward quadrant is produced when the nozzle is operated at non-ideally expanded conditions. Mach wave radiation propagates into the aft quadrant when the exhaust temperature is elevated. Subsequent tests in an acoustically treated nozzle thrust stand demonstrate the value of the near field array allowing immediate feedback on the noise/performance tradeoff for high speed jet noise reduction technologies.

NOMENCLATURE

a	speed of sound
C_t	thrust coefficient
C_i	eigenvector
D	nozzle diameter
F_1	stream thrust entering control volume
H_x	net axial thrust
H_2	axial balance output (force)
k	wavenumber
K_{ij}	Cross Spectral Matrix (CSM)
p(t)	unsteady pressure
P(ω)	Fourier transform of p(t)
NPR	nozzle pressure ratio - nozzle/ambient
S(ω)	Fourier transform of s(t)
TR	temperature ratio - nozzle total temperature/ambient
x	axial coordinate
y	lateral (radial) coordinate
$\|\lambda\|^2$	eigenvalue
ω	radian frequency

subscripts

a	ambient
1	metering station
2	seal station
m	lateral measurement location
p	lateral propagation location

1 INTRODUCTION

Part I of this paper (presented at this conference in 2009) demonstrated that a linear array of near field microphones can be used to assess the noise radiated to the far field using a procedure known as acoustic holography.[1] It was shown that both of the principal features of supersonic exhaust nozzles are present. Shock cell noise radiating in the forward quadrant is produced when the nozzle is operated at non-ideally expanded conditions. Mach wave radiation propagates into the aft quadrant when the exhaust temperature is elevated. The present activity serves to validate the near field array measurement for these features. This is a two step procedure. First the accuracy of the near field measurement and propagation process is demonstrated using simultaneous far field measurement in a high quality anechoic jet facility. Second is to identify facility issues that can arise from

* author of correspondence

differences such as flow profile, turbulence, and boundary layer characteristics and Reynolds number.[2]

Section 2 provides background for the mathematical propagation of the near field data to the far field using acoustic holography. Section 3 provides the array results using simultaneous far field measurement. Section 4 describes simultaneous near field noise and performance measurements in a thrust facility where far field measurements are not possible. A simple noise / performance tradeoff is conducted. A generic CD nozzle with a clean exit is compared to the same nozzle with small tabs or chevrons extending from the exit. The tabs reduce the far field noise by ~1 dB and "cost" ~0.1% thrust performance. The chevrons reduce noise by 2-3 dB and "cost" ~0.6% thrust performance. This data provides a reference for studies of future nozzle designs and alterations.

2 BACKGROUND FOR ACOUSTIC HOLOGRAPHY

Acoustic holography is used to propagate the measured nearfield pressure. The implementation used in this study differs from classical planar holography.[3] It is used with a linear array at a radial distance from the jet centerline rather than a 2D planar surface. It has been used in similar studies of exhaust noise. Subsonic jet noise is evaluated in tests similar to this program to aid the design tradeoffs for commercial turbofan engine exhaust systems. Shock cell noise at cruise conditions is evaluated in a transonic wind tunnel where it is important to account for the forward flight speed and the turbulent boundary layer traveling over the surface of the flush transducers.[4]

The procedure adopted here is often called Spatial Transformation of Sound Fields (STSF).[5] This relies on principal component analysis (the Singular Value Decomposition) to separate the measurement into orthogonal subspaces. The first step is to compute the full cross spectral matrix (CSM) as the outer product between all transducer pairs,

$$K_{ij}(\omega)=\frac{1}{m}\sum_{k=1}^{m} P_i(\omega)\,P_j^H(\omega)\ . \qquad \mathbf{1}$$

The next step is to divide the measured CSM into its fundamental fluctuation modes via Principal Component Analysis (PCA). Other names for this tool are The Proper Orthogonal Decomposition or the Karhunen-Loeve Expansion. This leads to a matrix eigenvalue equation,

$$K_{ij}C_{jn}=|\lambda_n|^2 C_{in}\ . \qquad \mathbf{2}$$

The eigenvalue λ^2 represents the energy content and the eigenvector C_i represents the characteristic signal form at the i_{th} transducer location. The signal portion of the n_{th} partial field spectrum can be identified as,

$$S^n(x;\omega)=\lambda_n C^n(x;\omega)\ . \qquad \mathbf{3}$$

Then, the signal S(ω) is "propagated" to a new radial distance using a propagation operator. This is done in the wavenumber domain obtained from the spatial Fourier transformation of S,

$$S(k_x,\omega)=\int S(x;\omega)\,e^{-ik_x x}\,dx\ . \qquad \mathbf{4}$$

In this equation k_x represents the wavenumber along the measurement axis. It should not be confused with the acoustic wavenumber $k_a=\omega/a$. The relationship between k_a, k_x, and k_y is described by the Pythagorean triangle,

$$k_y=\left[(\omega/a)^2-k_x^2\right]^{1/2}\ . \qquad \mathbf{5}$$

In fact, it is precisely the difference between k_x and k_a that allow the measurement radius, y_m, to be propagated to the desired radius, y_p, via the propagation operator,

$$S(k_x;y_p)=(y_m/y_p)^{1/2}S(k_x;y_m)e^{ik_y(y_p-y_m)}\ . \qquad \mathbf{6}$$

The first term provides the radial divergence and the second term provides the wave pattern due to the axial variations. The true functionality is based on a Hankel Function derived from the Bessel Function of the first and second kind, but this approximate equation is valid for all regions of interest outside the plume. This ensures that the total acoustic energy remains constant on all cylinders surrounding the jet axis. This yields an estimate of the spectrum at the new location y_p. The standard far field acoustic spectrum is found by conjugate multiplication S*S.

3 GE CELL 41 MEASUREMENTS

3.1 Exhaust Nozzle Geometry

A convergent-divergent (CD) exhaust nozzle is used to validate the near field array using simultaneous near field and far field measurements. The nozzle shown in Figure 1 has a throat diameter D=3.54 inches and area ratio A/A*=1.1. The internal geometry on the left is surrounded by the external nacelle shown on the right. An identical smaller nozzle is used in a second facility (Aero Systems Engineering Channel 8) described later in section 4. Comparison of these data sets allows facility differences to be separated from errors caused by the mathematical propagation process. This is called the array "calibration" although validation or verification may be more appropriate terminology.

Figure 1. Convergent-Divergent Exhaust Nozzle

3.2 GE Cell 41

Far field noise is measured in The GE Aircraft Engines Cell 41 anechoic free-jet noise facility shown in Figure 2. The inner surface of this cylindrical chamber is lined with anechoic wedges made of fiberglass wool to render the facility anechoic above 220 Hz. The facility is equipped with a traversing tower containing 13 microphones, mounted 22 ft off axis at polar angles from 45° to 155°. Model air is heated by direct vitiation and can be delivered at temperatures up to 1960 °R with nozzle pressure ratios up to 5.5.[6]

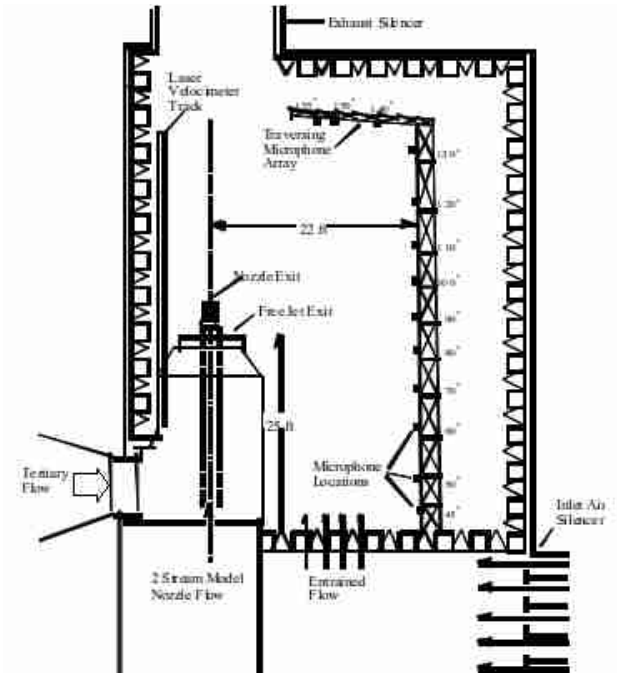

Figure 2. GE Cell 41 Test Facility

The near field array is installed parallel to the jet axis as shown in Figure 3. The array structure is 1 inch wide and the active length where transducers are installed extends 5 ft downstream from the nozzle exit. The measurement is made with piezoelectric pressure transducers flush mounted in the surface to prevent wind induced self noise. The boundary layer that grows on the surface produces pressure fluctuations that convect subsonically along the surface. These reactive fluctuations are filtered by the process described in Equation 6. At low frequency the flush mounting behaves like a free-field measurement because the acoustic wavelength is large compared to the size of the mounting surface. But, at high frequency the wavelength is small compared to the effective surface (1 inch wide and several inches long). This increases the level by up to 6 dB over the true free field.

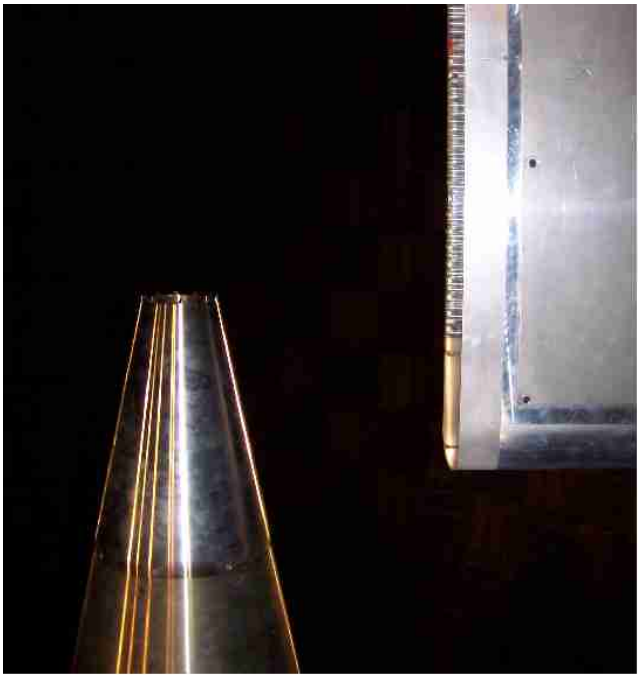

Figure 3. C41 Nozzle Installation

The geometry for the outward propagation of the near field noise is shown in Figure 4. Tests are conducted with the microphone array located at y=2D and y=3D from the jet centerline to demonstrate that the process is robust to the precise array location. The required spectral information is collected and appended with zeros in the upstream and downstream directions to cover the axial range of interest. The information is mathematically propagated outward to the location of the far field microphones. The far field noise measured at the tower location in Cell 41 is corrected to lossless conditions for direct comparison.

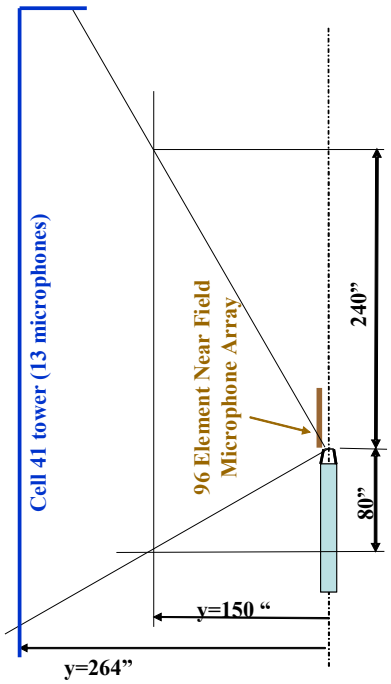

Figure 4. Geometry for Noise Propagation.

3.3 Cell 41 Test Results

A typical spectral result is shown in Figure 5. The vertical axis is given in band number =10log(Hz) which ranges from 250 Hz to ~50 kHz. The horizontal axis identifies the distance from the nozzle exit. Color bands indicate the 1/3 octave spectral level. Two significant physical features of the noise are identified. Shock cell noise is created by shear layer turbulence interacting with the basic shock cell pattern when the exhaust is imperfectly expanded. As the turbulence convects from one cell to the next a noise radiation pattern is produced by constructive and destructive interference.[7] This generates low frequency noise radiating in the upstream direction, and high frequency noise radiating toward the sideline and into the aft arc.[8] This noise is minimized when the nozzle is operated near full expansion. Mach wave radiation is created by the convection of turbulence at supersonic speeds. An instability wave model predicts the nominal radiation angle into the aft arc at ~140°.[9] This agrees with the measured angle to the center of the noise peak. It is present in all supersonic nozzle flows and is independent of whether or not the flow is perfectly expanded. In ambient temperature jets this source has the same level as the shock cell noise issuing from a convergent nozzle. But, at elevated temperature, which is the case of practical interest, this source is dominant. The similarity between parts a and b validates the near field propagation process.

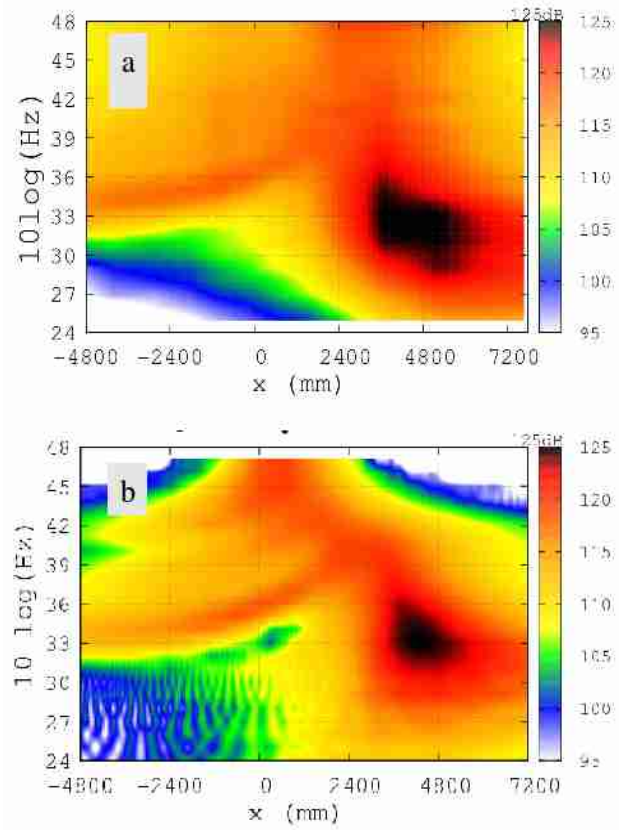

Figure 5. Far Field: A/A*=1.1, PR=4.0, TR=2.4, y/D=50
a - Actual Far Field b - Predicted from Near Field Array

Validation of the acoustic levels is done using the overall power shown in Figure 6. The ▼ and □ represent integration of the far field microphones (by independent methods) corrected to lossless conditions. The red symbols represent the integration of the near field array data that has gone through the holography process to eliminate the reactive portion of the measurement. The ● correspond to integration at the source location and the diamond at the far field location. Since the measurement is made close to the source it is assumed to be lossless. 65 test conditions were conducted on successive days. On day one: y=2D and RH=33%; on day two y=3D and RH=86%. The near field measurement results in the same far field level at most frequencies but there is a high frequency discrepancy suggesting an error in atmospheric attenuation (which is a strong function of humidity particularly when correcting to lossless conditions).[10] The remaining error between the far field and near field could be humidity, or it could be due to nonlinear propagation.[11] These discrepancies only affect the high frequencies where the noise level is well below the peak. They are interesting from an academic standpoint but do not affect any pragmatic trade-off decisions. Direct noise from the engine dominates this region.

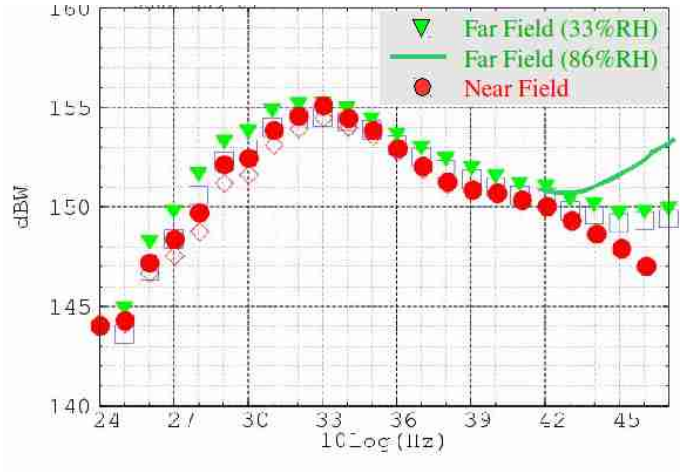

Figure 6. Acoustic Power: A/A*=1.1, PR=4.0, TR=2.4.

4 CHANNEL 8 TESTS

The Channel 8 acoustic configuration shown in Figure 7 is used to obtain noise and performance information up to NPR=5. Air from high pressure storage passes through a long-radius ASME metering nozzle to obtain the mass flow. The meter is located at the metric interface to provide the stream thrust entering the model control volume. Pressure and temperature rakes installed in the supply duct upstream of the model are used to set the test conditions. Nozzle thrust is determined from force measurement with a 3-component strain-gage force balance. The balance output consists of the axial force, normal force and the pitching moment. The nozzle is isolated from the facility piping by elastic seals at the metric interface.

The nozzle flow exhausts into the 53 inch diameter cabin lined with 3 inch deep foam wedges. The exhaust is powered by an ejector system to simulate forward flight up to M=0.3 through the 14 inch diameter free-jet. The exhaust system in includes a sonic "choke" to prevent noise from the ejector propagating forward into the test cabin. The nozzle exit plane is located adjacent to windows in the cabin for collecting shadowgraph images.

Temperature ratio up to TR~4 is simulated with a helium/air mixture which has been shown to replicate the essential physics of heated air.[12,13] The metered helium supply is mixed with the metered air supply upstream of the flow conditioning section to ensure mixing between the two streams.

Static performance tests at higher NPR typical of high speed cruise (NPR<20) can also be conducted but are not discussed in this paper. In this case the cabin is reconfigured and sealed at the upstream end eliminating the inlet freejet. The ejector reduces the cabin pressure to ~0.5 bar producing an increased NPR for the same nozzle total pressures.

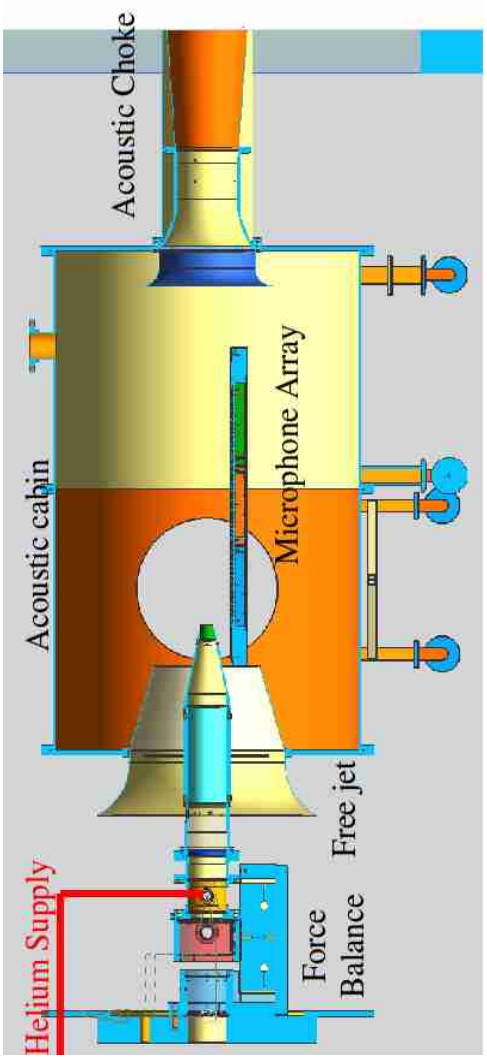

Figure 7. Test Facility for Noise/Performance Evaluation

Figure 8. CH8 Nozzle Installation

The acoustic tests in this facility use a nozzle with identical geometry to that used in Cell 41. The throat diameter is 2.25 inches corresponding to a scale ratio between the two nozzles of 1.58. The array installation shown in Figure 8 is similar to the installation in Cell 41 using flush mounted transducers to prevent wind induced self noise .

4.1 Acoustic Tests for A/A*=1.1

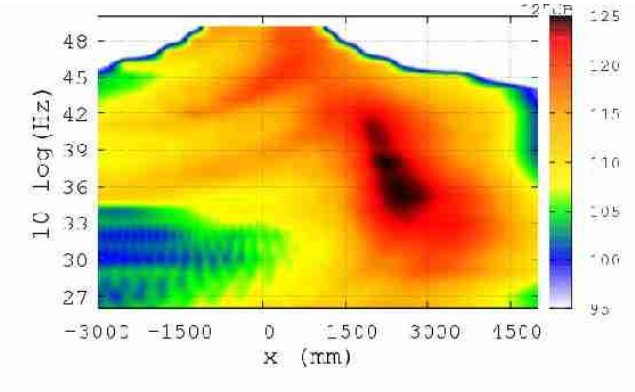

Figure 9. Noise Map: NPR=4.0, TR=2.4, y/D = 50

The noise map in Figure 9 is configured to the same conditions as the Cell 41 result shown in Figure 5. The 1.58 scale ratio causes an upward shift in the frequency from bands 24 - 48 for cell 41 to bands 26 – 50 for Channel 8. Part a shows the far field result with the axial range adjusted by the scale ratio for direct comparison with the Cell 41 result in Figure 5. The similarity between these maps is strong indication that the Channel 8 facility is able to reproduce the essential noise characteristics in spite the small size of the cabin.

Examples combining the data from both facilities show the acoustic power under different operating conditions. The Cell 41 result is adjusted by the scale ratio for direct comparison to the Channel 8 result. Figure 10 replicates the conditions in Figure 6. Figure 11 and Figure 12 include a far field correction to account for scattering and refraction caused by the free jet shear layer.[14] The slight difference between the open and filled symbols is caused by noise measured on the array that propagates outside the far field measurement range. The comparison between the ● and the ■ defines the accuracy of the near field measurement by direct comparison to the simultaneously measured far field data. Inspection of all data sets identifies the error in any 1/3 octave band to be less than ~2 dB and the error in overall power to be less than ~1 dB. Comparison of the ▲ to the ■ identifies additional error of ~1 dB due the facility differences. Relative accuracy when conducting back-to-back tests is considerably better allowing differences between similar nozzle configurations to be easily determined.

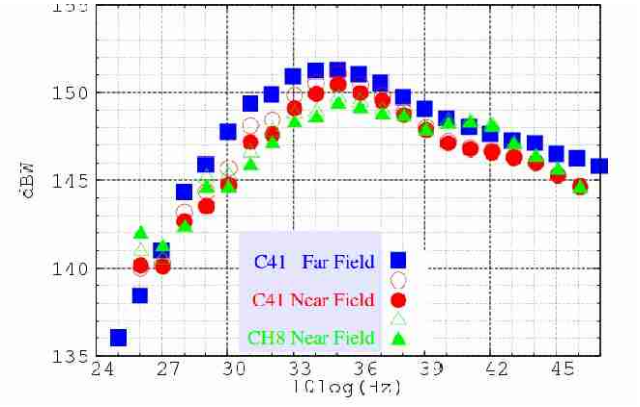

Figure 10. Acoustic Power: NPR=4.0, TR=2.4, M=0.0

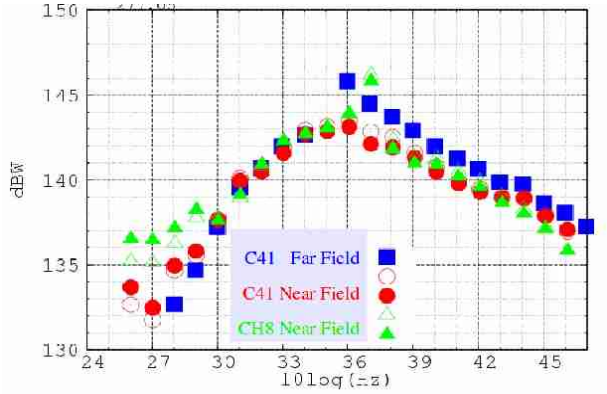

Figure 11. Acoustic Power: NPR=2.5, TR=2.4, M=0.12

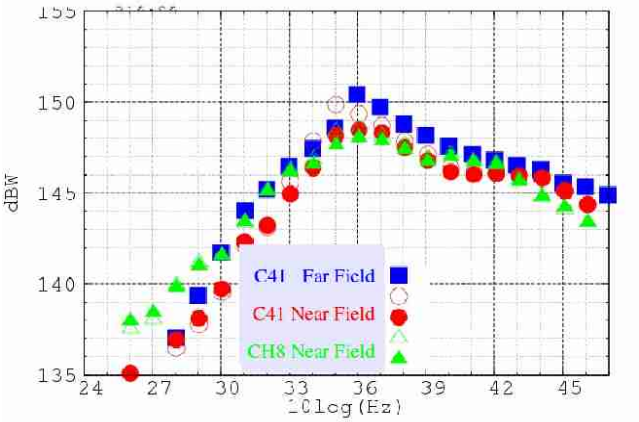

Figure 12. Acoustic Power: NPR=4.0, TR=2.4, M=0.22
Open symbols – integration at y=1D;
filled symbols – integration at far field

4.2 Noise / Performance Tradeoff for A/A*=1.2

The A/A*=1.2 nozzle shown in Figure 13 is used to evaluate the noise / performance tradeoff for tabs and chevrons extending from the nozzle exit. Two nozzle bodies are used to evaluate the effect of roughness on the expansion surface downstream of the nozzle throat. One has a smooth flow surface typical of the finish used on most scale model test articles. A simple boundary layer calculation starting at the throat suggests that the boundary layer at the nozzle exit is laminar. The other nozzle is designed to ensure that the exit boundary layer is fully turbulent. Cylindrical grooves are cut into the surface similar to threads on a machine screw. The depth of the thread is ~1% of the nozzle diameter. In terms of equivalent pipe flow this roughness is well into the fully rough regime. Three different nozzle exits (baseline, chevrons, or tabs) can be attached to either nozzle body allowing several combinations to be tested.

Figure 13. Nozzles for Noise / Performance Tradeoff

Before addressing the acoustic characteristics, the basic structure of the flowfield at A/A*=1.2 is identified using shadowgraph. Because the expansion surface is a simple conic section, compression and expansion waves will occur even when the flow is near the full expansion point. This is shown in Figure 14(a). These images are collected using ambient temperature with 40 msec exposure producing a clear image of the average flow structure. At this condition the flow is slightly underexpanded. Two sets of waves are evident. A wave originates at the nozzle lip due to the difference between the nozzle static pressure and the surrounding ambient. This produces a small Mach disk at the centerline and subsequently reflects from the shear layers as it travels down the plume. Another wave originates at the nozzle throat and exits the nozzle midway between the centerline and the wall. It also reflects off the shear layer creating an expansion/shock sequence traveling down the plume. There are two changes when the tabs or the chevrons are introduced. First is a slight shortening of the basic structure. Second is the appearance of axial streaks evolving from the devices.

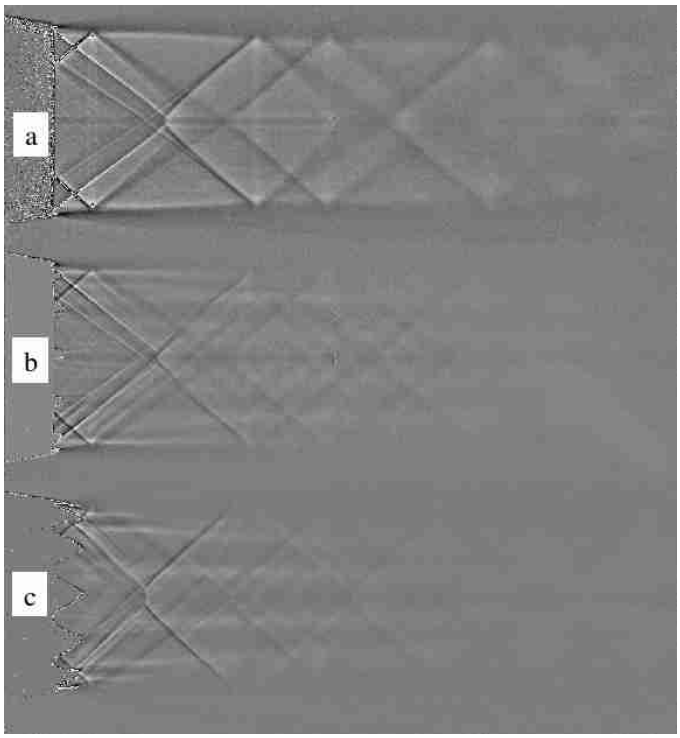

Figure 14. Shadowgraph, NPR=4.0:
a-Clean Exit, b-Tab Exit, c-Chevron Exit.

Care must be taken when using model scale experiments to identify the effect of nozzle geometry on noise production due to the potential for jet screech. This phenomena is not present in full scale engine exhaust flows and must be eliminated to make a proper assessment. This can be done by ensuring turbulent flow through the nozzle and is the reason for using the rough wall nozzle in Figure 13. An example of this effect is shown in Figure 15. The baseline nozzle with smooth contour and uniform low turbulence inlet flow shows the highest noise power at 2.5 kHz. Inspection of the noise maps for NPR=3.0 and NPR=3.5 show strong presence of screech at this frequency. The rough expansion shows similar noise levels at all conditions except NPR=3.5 where the level drops by 4 dB, indicating that the screech tone has been eliminated because of the turbulent boundary layer. Increasing the inlet freestream turbulence using a turbulence generator upstream of the nozzle throat eliminates the screech tone across the entire range.

With proper attention to eliminating screech, third octave power levels can be used to identify the gross effect of the geometric variations. Figure 16 corresponds to the A/A*=1.2 nozzle with rough expansion surface. The 4 kHz band is the dominant frequency of the Mach wave radiation. The symbol

◆ corresponds to the baseline nozzle. The effect of different nozzle extensions (tabs ▲, and chevrons ●) show a reduction in the acoustic power for NPR>2.7. This is qualitatively consistent with the presence of the turbulent streaks in Figure 14. The tabs show in increase in the axial turbulence and produce a slight noise reduction. The axial turbulence from the chevrons is greater with higher noise reduction. This trend is consistent with other programs involving chevron tests providing validity for the tests using the near field array.[1,15] All show a consistent noise reduction of 2-3 dB for chevrons when the flow conditions are underexpanded. At overexpanded conditions (NPR<2.7) the effect of the nozzle extensions is minimal because the adverse pressure gradient near the nozzle exit causes the boundary to thicken and possibly separate. Shadowgraph under these conditions show no evidence of axial streaks.

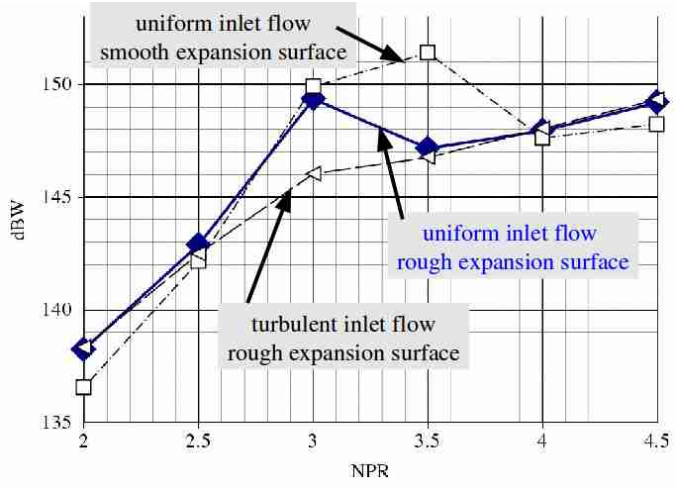

Figure 15. 1/3 Octave Acoustic Power, band 34 = 2.5 kHz

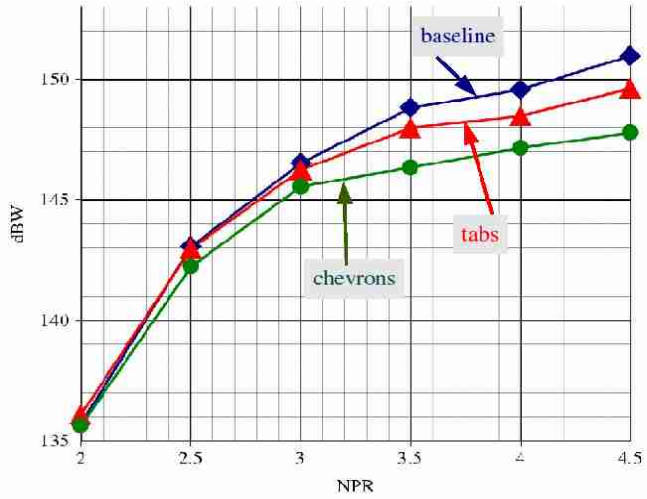

Figure 16. 1/3 Octave Acoustic Power, band 36 = 4.0 kHz

A complete evaluation of any nozzle system must include an assessment of the noise/performance tradeoff. The net static thrust, H_x, is determined by applying the momentum equation to the control volume surrounding the model,

$$H_x = F_1 + P_2 (A_2 - A_1) - P_a (A_2) - H_2. \qquad 7$$

The analysis of axial forces includes a balance force (H_2), pressure-area terms to account for the seal area, A_2, and the stream thrust, F_1, of the ASME metering nozzle at the interface between the grounded facility and the metric model. A calibrated elastic seal at the metric interface prevents force transmission to the facility. The thrust coefficient is found by dividing the net thrust in equation 7 by the ideal thrust from an inviscid calculation based on uniform flow at the nozzle exit. Scale model experiments typically use models of similar size to those used for acoustic studies. Consequently the boundary layer is often laminar or transitional rather than fully turbulent as would exist in a full scale engine. Most cases cause little difficulty for the performance assessment because the flow is accelerating toward the nozzle exit. The engineer simply replaces the skin friction from a scale model calculation with a turbulent boundary layer from the engine calculation. However, this adjustment can cause difficulty for a CD nozzle at supersonic conditions. For an underexpanded nozzle the flow continues to accelerate from the throat and there is little flow separation. In this case the conventional adjustment can be applied with confidence. The problem arises when the nozzle is overexpanded. In this case, flow separation within the nozzle is possible resulting in a corresponding reduction in thrust coefficient and some uncertainty in assessing the proper boundary layer conditions for applying corrections.

Figure 17 shows the effect of tabs and chevrons on the thrust. These curves are generated using a continuous sweep to cover the full NPR range of interest. The basic uncertainty of ΔC_t~0.002 is sufficient to characterize the effect. When required, higher accuracy can be achieved by collecting data at fixed conditions. The tab nozzle has similar thrust characteristics as the baseline except possibly for a slight reduction at underexpanded conditions. The difference however is within the error bands and fixed point operation would be required to confirm this conclusion. The effect of the chevrons is more pronounced showing a thrust reduction of ΔC_t~0.006.

The noise / performance tradeoff for the nozzle features shown in Figure 13 can be summarized. At underexpanded conditions the tabs reduce the acoustic power by ~1dB and cause a thrust reduction of ΔC_t~0.001. There is no effect on either noise or

performance at overexpanded conditions. The effect of the chevrons is more pronounced. There is a 2-3 dB noise reduction and a ΔC_t~0.006 thrust loss at underexpanded conditions. There is less effect at overexpanded conditions. It is likely that other chevrons designed by more sophisticated methods can achieve either higher noise reduction or a lower thrust loss. But these results provide a benchmark by which other designs can be evaluated.

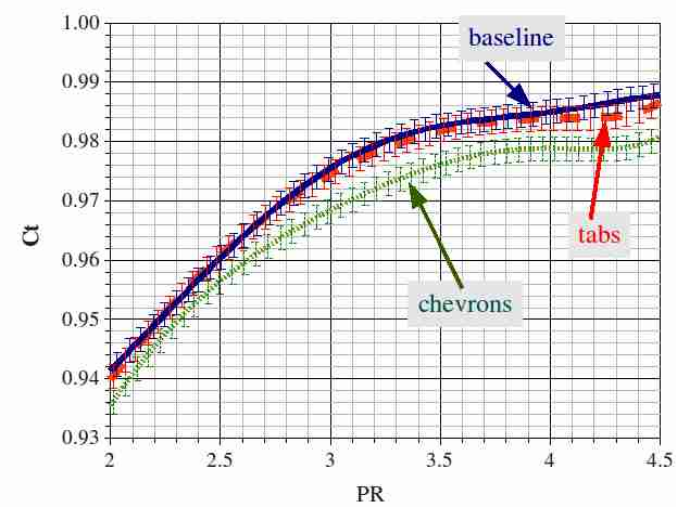

Figure 17. Thrust

5 CONCLUSION

A test program has been conducted to evaluate the noise/performance tradeoff for a typical convergent-divergent exhaust nozzle. Near field noise that is mathematically propagated to the far field compares favorably with actual far field measurements. This is significant because the near field measurement can be conducted simultaneously with corresponding performance tests in a thrust stand. The immediate feedback on the trade-off between noise and performance allows design iterations to be conducted efficiently.

Acknowledgement

Support for this work was provided by an SBIR program sponsored by NAVAIR Propulsion and Power.

6 REFERENCES

[1] Long, D., Martens S., "Simultaneous Noise and Performance Measurements for High Speed Jet Noise Reduction Technologies," ASME GT2009- 59073.

[2] Long, D., Maye. P., McDonald, T., "Effect of Inlet Flow Conditions on Noise and Performance of Supersonic Nozzles," AIAA-2010-3920, June, 2010.

[3] Maynard, J., Williams, E., Lee, Y., "Nearfield Acoustic Holography: I. Theory of generalized holography and the development of NAH," Journal of the Acoustical Society of America Vol. 78, Pp. 1395-1413, 1985.

[4] Long, D., "Evaluation of Jet and Shock Cell Noise via Acoustic Holography," AIAA paper 2008-0005, Jan 2008.

[5] K. B. Ginn and J. Hald, "STSF—Practical instrumentation and applications," Brüel & Kjær Technical Review 2, 1–27, 1989.

[6] Martens, S., Haber, L., "Jet Noise Reduction for High Speed Exhaust Systems," ASME – GT2008-50455.

[7] Harper-Bourne, M., Fisher, M., "The Noise from Shock Waves in Supersonic Jets," Agard CP #131, 1973, Pgs 11.1-11.13.

[8] Long, D., "The Structure of Shock Cell Noise from Supersonic Jets," AIAA paper 2005-2840, May 2005.

[9] Tam, C. "Supersonic Jet Noise," Annual Review Fluid Mechanics, Vol. 27, 1995, pgs 17-43.

[10] Shields, F., Bass, H., "Atmospheric Absorption of High Frequency Noise and Application to Fractional Octave Bands," NASA CR - 2760, 1977.

[11] Lee, S., Philip J. Morris, P.,Brentner, K., "Nonlinear Acoustic Propagation Predictions with Applications to Aircraft and Helicopter Noise" AIAA-2010-1384, January 2010.

[12] Papamoschou, D., "Acoustic Simulation of Coaxial Hot Air Jets Using Cold Helium–Air Mixture Jets, Journal of Power and Propulsion, Volume 23, No. 2, pgs 375-381, March 2007

[13] Kinzie, K.W., McLaughlin, D.K., "Measurements of Supersonic Helium/Air Mixture Jets," AIAA Journal, Vol. 37, No 11, 1999, Pg1363.

[14] Amiet, R., "Refraction of sound by a shear layer," Journal of Sound and Vibration 58 (1978), pp. 467.

[15] Henderson, B., "An MDOE Investigation of Chevrons for Supersonic Jet Noise Reduction," AIAA 2010-3926, June 2010.